

# 70 MW-level picosecond mid-infrared radiation generation by difference frequency generation in $\text{AgGaS}_2$ , $\text{BaGa}_4\text{Se}_7$ , $\text{LiGaSe}_2$ , and $\text{LiGaS}_2$

Michal Jelínek, Milan Frank, Václav Kubeček, Ondřej Novák, Jaroslav Huynh, Martin Cimrman, Michal Chyla, Martin Smrž, Tomáš Mocek

**Abstract**—Comparative study of nonlinear crystals for picosecond difference frequency generation in mid-IR is presented. Nonlinear crystals of  $\text{AgGaS}_2$ ,  $\text{BaGa}_4\text{Se}_7$ ,  $\text{LiGaSe}_2$ , and  $\text{LiGaS}_2$  were studied. In order to investigate the dependence of efficiency on the crystal length, three sets of crystals with lengths of 2, 4, or 8 mm were tested. The developed tunable DFG system was driven by the 1.03  $\mu\text{m}$ , 1.8 ps, Yb:YAG thin-disk laser system operated at the repetition rate of 10 or 100 Hz. As the best result, picosecond mid-IR pulses at a wavelength of  $\sim 7 \mu\text{m}$  with the energy up to 130  $\mu\text{J}$  corresponding to the peak power of  $\sim 72 \text{ MW}$  were generated using the 8 mm long  $\text{LiGaS}_2$  crystal. Using the  $\text{BaGa}_4\text{Se}_7$  crystal, DFG tunability in the wavelength range from 6  $\mu\text{m}$  up to 13  $\mu\text{m}$  was achieved.

**Index Terms**—Difference frequency generation, mid-infrared radiation, nonlinear optics, picosecond lasers.

## I. INTRODUCTION

Sources of coherent radiation in a mid-infrared (IR) spectral range ( $\sim 3\text{--}20 \mu\text{m}$ ) are interesting for many possible applications in vibrational spectroscopy, medicine (soft tissue ablation), biology (interaction with tissue or analysis), high-harmonic generation, attosecond science, atmospheric studies, etc. [1], [2]. Laser radiation around  $\sim 3 \mu\text{m}$  can be generated by well-developed  $\text{Er}^{3+}$ -doped lasers. Laser-diode pumped, quasi-continuous wave (QCW) lasers with  $>50 \text{ W}$  of average output power are commercially available. Several works are also devoted to a development of  $\text{Er}^{3+}$ :ZBLAN fiber lasers in continuous wave (CW) or Q-switched regime [3], [4]. Nevertheless, not all temporal regimes are readily available and mainly stable mode-locked operation for ultrashort pulse generation is still challenging.

Going farther into the infrared region, laser radiation can be generated directly by some special solid-state lasers based on  $\text{Fe}^{2+}$  or  $\text{Dy}^{3+}$  active ions. Lasers based on  $\text{Dy}^{3+}$ : $\text{PbGa}_2\text{S}_4$  can generate radiation at narrow spectral lines

around 4.3 or 5.4  $\mu\text{m}$  [5].  $\text{Fe}^{2+}$ -based lasers can provide generally continuously-tunable radiation in a wide spectral range because of strong interaction of the electronic states with lattice vibrations. Pumping of such lasers is generally not trivial because the  $\text{Fe}^{2+}$  absorption band is located around 3  $\mu\text{m}$ . Moreover, upper-state level lifetime at room temperature is in the order of hundreds of nanoseconds indicating special requirements on pumping sources. Therefore,  $\text{Er}^{3+}$ -based lasers, usually operated in a Q-switched regime, are usually used as pumping sources of  $\text{Fe}^{2+}$ -based lasers. Host materials such as ZnSe or ZnS were studied extensively and the tuning range of  $\sim 3.7$  to 5.3  $\mu\text{m}$  was presented [6], [7]. It has to be noted that the  $\text{Fe}^{2+}$  lifetime as well as fluorescence spectra and resulting tunability range are strongly influenced by the active material temperature. The spectral tuning range can be extended using other  $\text{Fe}^{2+}$  host materials such as CdTe or  $\text{Cd}_{1-x}\text{Mn}_x\text{Te}$  and pumping of such lasers by other  $\text{Fe}^{2+}$ :ZnSe lasers [8]. For example, smooth tunability of a  $\text{Fe}^{2+}$ :CdTe laser in the range  $\sim 4.5$  to 6.8  $\mu\text{m}$  was demonstrated [9]. Concerning other temporal regimes, CW  $\text{Fe}^{2+}$ :ZnSe laser generation was achieved and mode-locked regime in the sub-picosecond time domain was also successfully reported [10]. Some of these lasers became commercially available recently.

Moreover, there are commercially available and highly developed gas lasers based on CO or  $\text{CO}_2$  generating within the wavelength ranges of 5.2–6.0  $\mu\text{m}$  or 9.1–10.9  $\mu\text{m}$ , respectively. These lasers can be operated in various temporal regimes from CW to ultrashort pulse generation [11], [12]. Free-electron lasers represent another type of very versatile and broadly-tunable mid-IR radiation sources, but they suffer from complexity and costs [13]. These devices generate in a unique temporal regime. The generated macropulse with a duration of several  $\mu\text{s}$  consists of a  $\sim\text{GHz}$  train of micropulses with  $\sim 1 \text{ ps}$  duration. Semiconductor (quantum cascade) lasers present other interesting and applicable alternatives with CW output power at a level of several Watts [14], [15]. Generation of low average power sub-picosecond pulses was also presented recently [16]. There are also other alternative approaches for generation in mid-IR, for example, hydrogen Raman lasers [17].

An extensive group of applicable and highly versatile sources is based on nonlinear optical parametric processes. This concept has a great advantage in possibility of output wavelength tunability in a wide range given by the phase-matching conditions. There are generally several

Manuscript received October 10, 2024

Corresponding author: Michal Jelínek: michal.jelinek@tjfi.cvut.cz

Michal Jelínek, Milan Frank, and Václav Kubeček are with Czech Technical University in Prague, Faculty of Nuclear Sciences and Physical Engineering, Brehova 7, Prague, Czech Republic

Ondřej Novák, Jaroslav Huynh, Martin Cimrman, Michal Chyla, Martin Smrž, and Tomáš Mocek are with HiLASE Centre, FZU - Institute of Physics of the Czech Academy of Sciences, Za Radnicí 828, Dolní Brezany, Czech Republic

This work was co-funded by the European Union and the state budget of the Czech Republic under the project LasApp CZ.02.01.01/00/22\_008/0004573 and by "Center of Advanced Applied Sciences" (No. CZ.02.1.01/0.0/0.0/16\_019/0000778).

approaches: optical parametric generation (OPG), optical parametric amplification (OPA), optical parametric oscillation (OPO), and difference frequency generation (DFG) that can be considered as a special type of OPA. These individual methods are commonly combined in some multi-stage systems (OPG+OPA, OPG+DFG etc.) enabling the generation of longer wavelengths or higher energies. While OPG, OPA, and DFG can be essentially considered as single pass, OPO systems are based on multi-pass round-trip inside an optical resonator. Therefore, quality of an output beam generated by OPOs is generally better, usually close to a fundamental mode, and also the operation threshold is lower. In contrast to OPG or OPA systems, peak powers and energies generated by OPOs are orders of magnitude smaller.

DFG process, also known as parametric down-conversion, allows conversion of high-energy, visible or near-IR laser radiation into a mid-IR region or even further to THz frequency band [1], [18]–[20]. Concerning more closely on mid-IR region, this concept has been proven in a wide temporal range from CW [21] to pulsed regime with pulse duration from nanoseconds down to femtoseconds [22]. As DFG is a three-wave mixing nonlinear process, the nonlinear crystals have to be non-centrosymmetric, i.e. present the second order nonlinearity  $\chi^{(2)}$ . A choice of the nonlinear crystal depends on several factors and the desired wavelength belongs to the most important. Oxide crystals, as for example BBO ( $\text{BaB}_2\text{O}_4$ ), KTP ( $\text{KTiOPO}_4$ ), or  $\text{LiNbO}_3$  are widely used. Moreover, many of these crystals can be periodically-poled in order to increase conversion efficiency. On the other hand, their transparency range is limited, i.e. up to  $\sim 2.9 \mu\text{m}$  in the case of BBO, up to  $\sim 4.3 \mu\text{m}$  for KTP, or up to  $\sim 5.5 \mu\text{m}$  for  $\text{LiNbO}_3$  [23]–[25].

In order to develop efficient frequency converters into wavelengths longer than  $5 \mu\text{m}$ , non-oxide crystals should be employed because of their wider transparency range up to  $\sim 20 \mu\text{m}$  in some cases. Generally, sulphide-, selenide-, or phosphide-based crystals can be used and huge effort has been made to fabricate and investigate such crystals having acceptably high effective nonlinear optical coefficient ( $>5 \text{ pm/V}$ ) and reasonably high optical damage threshold [18]. Quasi-phase-matched (QPM), orientation-patterned (OP) semiconductors as OP-GaAs present other interesting possibilities; nevertheless, dimensions of such structures are limited by the fabrication process.

Moreover, because of two-photon absorption at  $\sim 1 \mu\text{m}$ , materials such as GaAs or GaSe have to be usually driven at  $>1.5 \mu\text{m}$  presenting a limiting factor for available pumping sources [26], [27]. A similar situation in terms of available pumping sources applies for crystalline  $\text{ZnGeP}_2$  (ZGP) also.

Concerning more closely on DFG systems excited by pulses at the wavelength of  $\sim 1 \mu\text{m}$ , many works were devoted to nanosecond pumping. For example, 10-ns pulses with the peak power of 3 kW at  $7.9 \mu\text{m}$  were generated using a  $\text{BaGa}_4\text{Se}_7$  (BGSe) crystal [28]. In order to achieve orders of magnitude higher peak power, excitation by shorter pulses in a picosecond range can be used.

Several other works concerning this approach based on the BGSe crystals were published. Using this crystal driven by a 30 ps Nd:YAG laser, output energy of 140-230  $\mu\text{J}$  at 8-14  $\mu\text{m}$

with the peak power of up to  $\sim 7 \text{ MW}$  has been achieved [29]. Moreover, the highest peak power of  $\sim 27 \text{ MW}$  at  $3.9 \mu\text{m}$  (energy of 830  $\mu\text{J}$  in 30 ps pulses) was generated under similar pumping conditions [30]. Using  $\text{LiInS}_2$  (LIS) crystal driven by a 25 ps Nd:YAG laser, output energy of 350  $\mu\text{J}$  at  $5.4 \mu\text{m}$  corresponding to the peak power of up to  $\sim 14 \text{ MW}$  has been demonstrated [2]. Our group has also presented preliminary results on BGSe under 1.8 ps pumping in [31]. Using  $\text{LiGaS}_2$  and  $\text{LiGaSe}_2$  crystals it was possible to generate up to 50  $\mu\text{J}$  energy level in the 4.6-10.8  $\mu\text{m}$  wavelength range with the peak power of up to  $\sim 2.5 \text{ MW}$  under pumping by a  $1.064 \mu\text{m}$ , 20 ps Nd:YAG laser [32].

There is also a growing number of works devoted to intrapulse difference frequency generation (iDFG) in a timescale of tens of femtoseconds [33]–[37]. This method is generally versatile, simple, and robust. On the other hand, generated mid-IR pulse energy is comparatively low. In order to generate such pulses at  $\sim \mu\text{J}$  energy level, it is useful to incorporate amplifier stages. For example, a developed system extended by two OPA stages based on  $\text{LiGaS}_2$  enabling to generate 6  $\mu\text{J}$ ,  $\sim 100 \text{ fs}$  pulses at  $\sim 6 \mu\text{m}$  was demonstrated [34].

We have developed a system generating between these two temporal ranges, i.e. pulses in a picosecond scale. Mid-IR pulses with the energy up to 130  $\mu\text{J}$  corresponding to the peak power of  $\sim 72 \text{ MW}$  were generated. Using various nonlinear crystals, tunability in the wavelength range from 5 up to 13  $\mu\text{m}$  was achieved. Comparative study of  $\text{AgGaS}_2$  (AGS),  $\text{BaGa}_4\text{Se}_7$  (BGSe),  $\text{LiGaS}_2$  (LGS), or  $\text{LiGaSe}_2$  (LGSe) with various lengths was performed. The developed DFG system was driven by the  $1.03 \mu\text{m}$ , 1.8 ps, Yb:YAG thin-disk based Perla B laser system at the HiLASE centre [24].

## II. EXPERIMENTAL SETUP

The fundamental optical layout of the designed DFG system is presented in Fig. 1. The principal idea of this setup was proposed in [38]. Additional lenses were used in the setup in order to optimize beam spot size on the SHG, OPG, and DFG elements.

Notation in the order of pump – signal – idler ( $\lambda_{\text{pump}} < \lambda_{\text{signal}} < \lambda_{\text{idler}}$ ) will be used in the following descriptions of three-wave mixing processes. The  $1.03\text{-}\mu\text{m}$  laser with maximum pulse energy of 11 mJ was used as a pump source for a double-stage frequency-converter into the mid-IR region. According to the autocorrelation measurement, the pulse duration was 1.8 ps assuming  $\text{sech}^2$  pulse shape. The spectral bandwidth was  $\sim 1.5 \text{ nm}$  indicating that the pulse was not fully transform-limited.

The laser output energy was adjustable using a motorized attenuator and the pulse repetition rate was reduced from 1 kHz down to 10 Hz by a pulse picker during most of the experiments. Furthermore, the setup with the 8 mm long BGSe crystal was tested at the highest output energy at the pump repetition rate of 100 Hz without any damage nor DFG output characteristics decrease. This result confirms that further mean output power scaling is possible.

The first stage was a generator of a signal wave for DFG based on a double pass optical parametric generator - amplifier

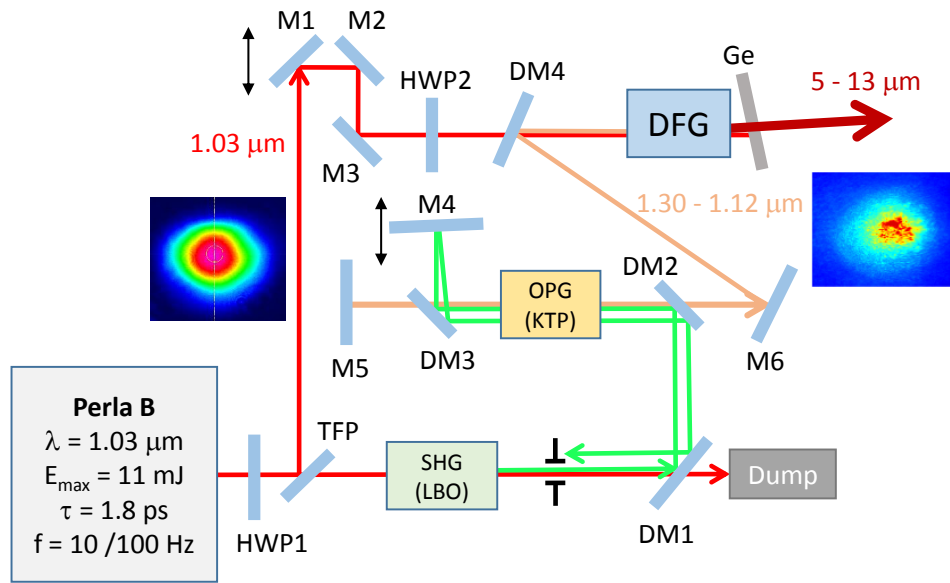


Fig. 1. Optical layout of the DFG system in collinear geometry. SHG: second harmonic generator, OPG: optical parametric generator, DFG: difference frequency generator. TFP: Thin film polarizer; HWP: half-wave plate @  $1030 \text{ nm}$ ; M1, M2, M3: HR @  $1030 \text{ nm}$ ; M4: HR @  $515 \text{ nm}$ ; M5 and M6: HR @  $1100\text{-}1300 \text{ nm}$ . DM: dichroic mirrors: DM1: HR @  $515 \text{ nm}$ , HT @  $1030 \text{ nm}$ ; DM2 and DM3: HR @  $515 \text{ nm}$ , HT @  $1100\text{-}1300 \text{ nm}$ ; DM4: HR @  $1120\text{-}1270 \text{ nm}$ , HT @  $1030 \text{ nm}$ . Ge: Germanium plate used to block pump as well as signal radiation. Insets: spatial profiles of pump and signal beams. Additional lenses used for optimization of the beam spot sizes are not shown for better clarity.

(OPG - OPA) system driven by a second harmonic generation (SHG) stage. Generated idler wave (tunable in a range of  $\sim 1.12$  to  $1.30 \mu\text{m}$ ) was used as a signal wave for the DFG stage. DFG was studied in several nonlinear crystals described in section III. The horizontally polarized pump beam ( $1.03 \mu\text{m}$ ) and vertically polarized signal beam ( $\sim 1.12$  to  $1.30 \mu\text{m}$ ) were combined in the type II DFG crystal. A delay stage formed by the mirrors M1-M2 was used in the pump beam for precise adjustment of the temporal overlap between the pump and signal beam. The HWP2 was used to adjust the correct polarization of the pump wave for DFG.

Details of the first stage of the frequency conversion system are following: The SHG was based on an LBO crystal with a length of  $5 \text{ mm}$ , aperture of  $5 \times 5 \text{ mm}^2$ , cut at  $\Theta = 90^\circ$ ,  $\varphi = 13^\circ$ , anti-reflection-coated (AR) at  $515 \text{ nm}$  and  $1030 \text{ nm}$ . During the DFG measurements described later, HWP1 was used to keep excitation pulse energy for the SHG crystal at a constant level of  $2.2 \text{ mJ}$ . This value was limited by the damage threshold under given conditions. Therefore, signal pulse energy for DFG was also kept at a constant level while pump pulse energy for DFG was varied during these measurements. Residual  $1.03 \mu\text{m}$  radiation was transmitted through DM1 into a beam dump. SHG radiation at  $515 \text{ nm}$  served as excitation for the OPG-OPA system. It was based on a KTP crystal with a length of  $5 \text{ mm}$ , aperture of  $10 \times 10 \text{ mm}^2$ , cut at  $\Theta = 73^\circ$ ,  $\varphi = 0^\circ$ , AR at  $900\text{-}1400 \text{ nm}$ , for  $o \rightarrow eo$  interaction (pump  $\rightarrow$  signal, idler). During the first pass through the KTP, a spectrally-broadband ( $>30 \text{ nm}$ ) and spatially-divergent conical idler beam was generated. It was transmitted through DM3 and reflected back into the KTP by M5. The pump beam at  $515 \text{ nm}$  was reflected by DM3 and further reflected back into the KTP by M4. M4 was placed on a precise translation

stage in order to adjust the temporal overlap between the pump and idler beams in the KTP during the second pass. The path of the back-reflected pump at  $515 \text{ nm}$  was slightly misaligned in the horizontal plane by M4 and therefore the back-reflected pump can be blocked by an iris placed in front of the SHG crystal. Using this second pass, the idler beam was amplified as well as spectrally and spatially narrowed. This idler beam was further transmitted through DM2 and directed into the DFG crystal. The idler wave generated by this OPG-OPA system was tunable in the wavelength range of  $1.12$  to  $1.30 \mu\text{m}$  by slight rotation of the KTP crystal. The spectral full-width at half-maximum (FWHM) was  $10 \text{ nm}$  and the maximum generated energy of  $\sim 25 \mu\text{J}$  was limited by the KTP damage threshold. The spatial profile is presented in the inset of Fig. 1. It has to be noted that there was also a shorter (signal) wave generated around  $0.93 \mu\text{m}$  also but it was not used for further experiments and it was transmitted through DM4.

Nonlinear crystals used in the second stage of the frequency conversion are described in section III in detail. The pump beam spatial profile was approximately Gaussian with an average diameter of  $2.8 \text{ mm}$  (measured at  $1/e^2$ ) in the place of the DFG crystal. The calculated effective area of  $3.1 \text{ mm}^2$  was used for further energy density calculations in accordance with the ISO standard 21254-1. A smaller pump beam may lead to higher conversion efficiencies at lower pump energies, but the main objective of this work was to use the maximum available pumping energy and generate as high mid-IR energy as possible without the DFG crystal damage. The signal beam diameter in the place of the DFG crystal was about  $1.6 \text{ mm}$ .

### III. NONLINEAR CRYSTALS FOR MID-IR DIFFERENCE FREQUENCY GENERATION

DFG was investigated in nonlinear crystals of AGS, BGSe, LGS, and LGSe. Overview of all investigated samples is presented in Table I together with fundamental crystallographic properties. Length of the samples was in the range between 1 and 8 mm. Some of the crystals were anti-reflection (AR) coated at 1.2-1.5  $\mu\text{m}$ . Nonlinear characteristics of the crystals were calculated using SNLO [25]. The crystals were cut at the angles ( $\Theta$ ,  $\varphi$ ) enabling access to a reasonably high effective nonlinear optical coefficient  $d_{\text{eff}}$  for the selected type of interaction at the following central wavelengths: pump 1.03  $\mu\text{m}$ , signal 1.20  $\mu\text{m}$ , idler 7.27  $\mu\text{m}$ . It has to be noted that magnitudes of nonlinear optical coefficients used in SNLO for BGSe are somewhat uncertain and several papers presenting novel data were published recently [39], [40]. On the other hand, values of  $d_{\text{eff}}$  for AGS, LGS, and LGSe have been validated with the same results in many publications. Phase-matching curves are presented in Fig. 2.

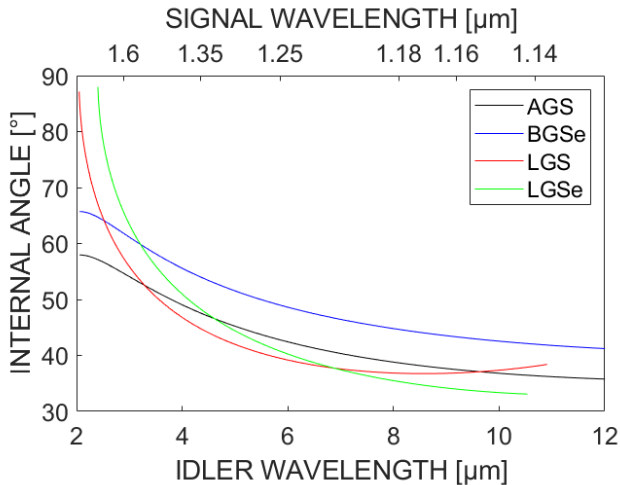


Fig. 2. Calculated phase-matching curves of AGS, BGSe, LGS, and LGSe crystals for collinear setup in principal planes according to Tab. I.

Unpolarized transmission spectra of these crystals were measured using a spectrophotometer (Shimadzu UV-3600) and an FT-IR spectrometer (Nicolet). Fresnel reflections were subtracted, spectral dependencies of the net absorption coefficient were calculated and they are presented in Fig. 3. Slight noise at  $\sim 4.3$   $\mu\text{m}$  is essentially caused by  $\text{CO}_2$  absorption and noise around 6.4  $\mu\text{m}$  is caused by water vapor absorption. These data are in a good agreement with SNLO [25]. It can be seen that the absorption coefficient increases significantly (higher than  $2 \text{ cm}^{-1}$ ) above  $\sim 9.0$   $\mu\text{m}$  for LGS, above  $\sim 10.6$   $\mu\text{m}$  for LGSe, above  $\sim 11.9$   $\mu\text{m}$  for AGS, and above  $\sim 17$   $\mu\text{m}$  for BGSe.

### IV. CHARACTERISTICS OF MID-IR DIFFERENCE FREQUENCY GENERATION

Laser-induced damage threshold (LIDT) was measured using same pump laser system but slightly different beam spot sizes in some cases. Input surface damage was observed at pump pulse energy densities of approximately 0.16 and

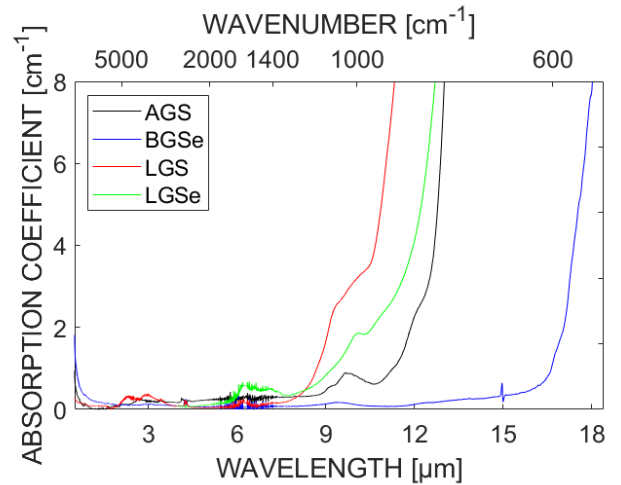


Fig. 3. Spectral dependencies of net absorption coefficients for AGS, BGSe, LGS, and LGSe.

$0.21 \text{ J/cm}^2$  for the AR-coated BGSe and LGSe crystals, respectively. In order not to damage other crystals, the energy density was kept slightly lower during the following DFG measurements. Although these measured values are not fully comparable with the values published for the uncoated crystals, they present a good estimation for further measurements. The uncoated AGS and LGS crystals were not damaged by the pump energy density of 0.15 and  $0.23 \text{ J/cm}^2$ , respectively.

Mid-IR single pulse energy generated by the DFG system operated at 10 Hz was measured by a sensitive energy probe (Coherent J10MB-LE). When the system was operated at 100 Hz, the single pulse energy was measured by the energy probe and also mean power was measured by a power meter (Thorlabs PM16-401). The single pulse energy was calculated from this power measurement and the values are in good agreement.

Characteristics of generated pulse energy and energy conversion efficiency of the output radiation at the wavelength of  $\sim 7$   $\mu\text{m}$  as a function of the pump pulse energy for all investigated crystals are presented in Fig. 4. This wavelength was chosen because of the crystals cut as well as limited LGS transmission range. Germanium filter transmittance was taken into account, i.e. the presented values are in front of this filter. All crystals were tested up to the pump energy density close to the limit given by the LIDT value. It has to be also noted that the 8 mm long LGSe crystal was partially damaged during previous experiments that might negatively affect the output energy. The highest output energy of 130  $\mu\text{J}$  with the conversion efficiency of 2% was achieved using the 8 mm long LGS crystal for the pump energy of 6.7 mJ corresponding to energy density of almost  $0.2 \text{ J/cm}^2$ . Assuming the output pulse duration comparable to the pump pulse duration of 1.8 ps, the peak power exceeded 72 MW level. It has to be noted that for the highest pump level, the optimal signal energy might be higher, but it was limited by the OPG/OPA performance. Maximum conversion efficiency for this crystal was 2.5% at lower pump energy of 3 mJ. Using the 8 mm long BGSe

TABLE I  
OVERVIEW OF THE INVESTIGATED DFG CRYSTAL SAMPLES.

	AGS	BGSe			LGSe			LGS		
Anisotropy	neg. uniax.	biaxial			biaxial			biaxial		
Class	42m	m			mm2			mm2		
DFG interaction type	1	1			2			2		
Pump-Signal-Idler	ooo	oeo			eoe			eoe		
Principal plane	-	XZ			XY			XY		
$\Theta; \varphi$	$34^\circ; 45^\circ$	$45^\circ; 0^\circ$			$90^\circ; 34^\circ$			$90^\circ; 39^\circ$		
$d_{\text{eff}}$ , pm/V	10.5	27			9.2			5.6		
Length, mm	2	1	4	8	2	4	8	2	4	8
Aperture, mm <sup>2</sup>	$8 \times 5$	$4 \times 4$	$5 \times 5$	$5 \times 6$	$4 \times 4$	$4 \times 4$	$4 \times 4$	$5 \times 5$	$4 \times 4$	$4 \times 4$
AR coating	no	no	no	yes	yes	yes	yes	no	no	no

crystal, the highest output energy was 120  $\mu\text{J}$  for pump energy of 5.1 mJ with the conversion efficiency of 2.3%. It should be also noted that at low pump energy of 1 mJ, the output energy was about 50  $\mu\text{J}$  and the conversion efficiency reached 5%. Using the 8 mm long LGSe crystal, the highest output energy was 60  $\mu\text{J}$  with the conversion efficiency of 1.4%. Using shorter crystals, the output energies were generally lower. In the case of 4 mm long crystals, the maximum output energy was  $\sim 100 \mu\text{J}$  for the LGS and LGSe crystals, and  $\sim 60 \mu\text{J}$  for the BGSe crystal. The conversion efficiencies were up to 2.5% in the case of LGSe crystal for pump energy of 2.5 mJ. In the case of 1 or 2 mm long crystals, the maximum output energy was 45  $\mu\text{J}$  for the 2 mm long LGSe crystal. Using the 2 mm long LGS, 2 mm long AGS, and 1 mm long BGSe crystals, the maximum output energy was comparable at a level of 25  $\mu\text{J}$ . The maximum conversion efficiency was 1% for the 2 mm long LGSe crystal. Shot-to-shot energy stability at high pump energy level was less than  $\pm 5\%$ .

Presence of energy roll-off effect was observed for longer crystals or crystals with higher nonlinear coefficients. This phenomenon is probably given by re-conversion of the idler wave back into the pump and signal waves. Solid lines in the graphs present results of numerical modeling based on SNLO [25] taking into account the spatial distribution with diffractive effects. It has to be noted that a shorter interaction length was used in this numerical modeling, taking into account non-optimal spatial or temporal overlap of the pump and signal beams. According to the simulation, in the ideal case for the 8 mm long crystals, the maximum output energy would be about 2 times higher.

The generated spectra in the mid-IR region were measured using a single grating monochromator (Oriel model 77250 with 77302 grating covering the spectral range 4-16  $\mu\text{m}$ , 75 lines/mm) together with a cryogenically-cooled mercury cadmium telluride (MCT) photodetector (Judson-Teledyne J15D12, spectral range 3-13  $\mu\text{m}$ ). Spectral resolution was on the order of 30 nm. The signal wave at the desired wavelength for DFG was tuned by the KTP crystal rotation, and the DFG crystal was rotated correspondingly in order to match the phase-matching condition.

Examples of the spectra generated by DFG using the 8 mm long BGSe and LGS crystals are presented in Fig. 5. In the case of the BGSe crystal, tunability in the range from  $\sim 6.5$  to 13  $\mu\text{m}$  was achieved. Shorter wavelengths might possibly be generated, but effort has been made to investigate

a long-wavelength spectral part. The spectral width (FWHM) ranged from 80  $\text{cm}^{-1}$  at  $\sim 7 \mu\text{m}$  to 40  $\text{cm}^{-1}$  at  $\sim 12.7 \mu\text{m}$ . It has to be noted that it was not possible to measure longer wavelengths than  $\sim 13 \mu\text{m}$  because of the MCT photodetector sensitivity limit. Using the 8 mm LGS crystal, the overall tunability range was  $\sim 5.3$  to 8.3  $\mu\text{m}$  and the long-wavelength part was probably limited by the crystal transmittance. The spectral width was ranging from 70  $\text{cm}^{-1}$  at  $\sim 5.5 \mu\text{m}$  to 80  $\text{cm}^{-1}$  at  $\sim 8 \mu\text{m}$ .

## V. DISCUSSION AND CONCLUSION

A comparative study of nonlinear crystals for picosecond difference frequency generation in the mid-IR was presented. Crystals of  $\text{AgGaS}_2$ ,  $\text{BaGa}_4\text{Se}_7$ ,  $\text{LiGaSe}_2$ , and  $\text{LiGaS}_2$  with various lengths were used. The developed tunable DFG system was driven by the 1.03  $\mu\text{m}$ , 1.8 ps, Yb:YAG thin-disk laser system operated at a repetition rate of 10 or 100 Hz. Picosecond mid-IR pulses at a wavelength of  $\sim 7 \mu\text{m}$  with energy up to 130  $\mu\text{J}$  corresponding to the peak power of  $\sim 72 \text{ MW}$  were generated using the 8 mm long  $\text{LiGaS}_2$  crystal. Using various nonlinear crystals, DFG tunability in the wavelength range from  $\sim 6$  up to 13  $\mu\text{m}$  was achieved. In agreement with simulation results, higher conversion efficiency up to 5% can be achieved for low pump energy densities using crystals with higher  $d_{\text{eff}}$  (BGSe or LGSe). On the other hand, at high pump energy densities approaching the crystal damage threshold, the conversion efficiency of 1 to 2% is comparable for all crystals due to strong reconversion. Longer crystals (4 or 8 mm) are beneficial for higher achievable maximum generated energy for the investigated pump pulse duration.

Yb:YAG thin-disk pump laser allows further increase of the output pulse repetition rate up to 1 kHz and therefore average output power scalability of the whole DFG system.

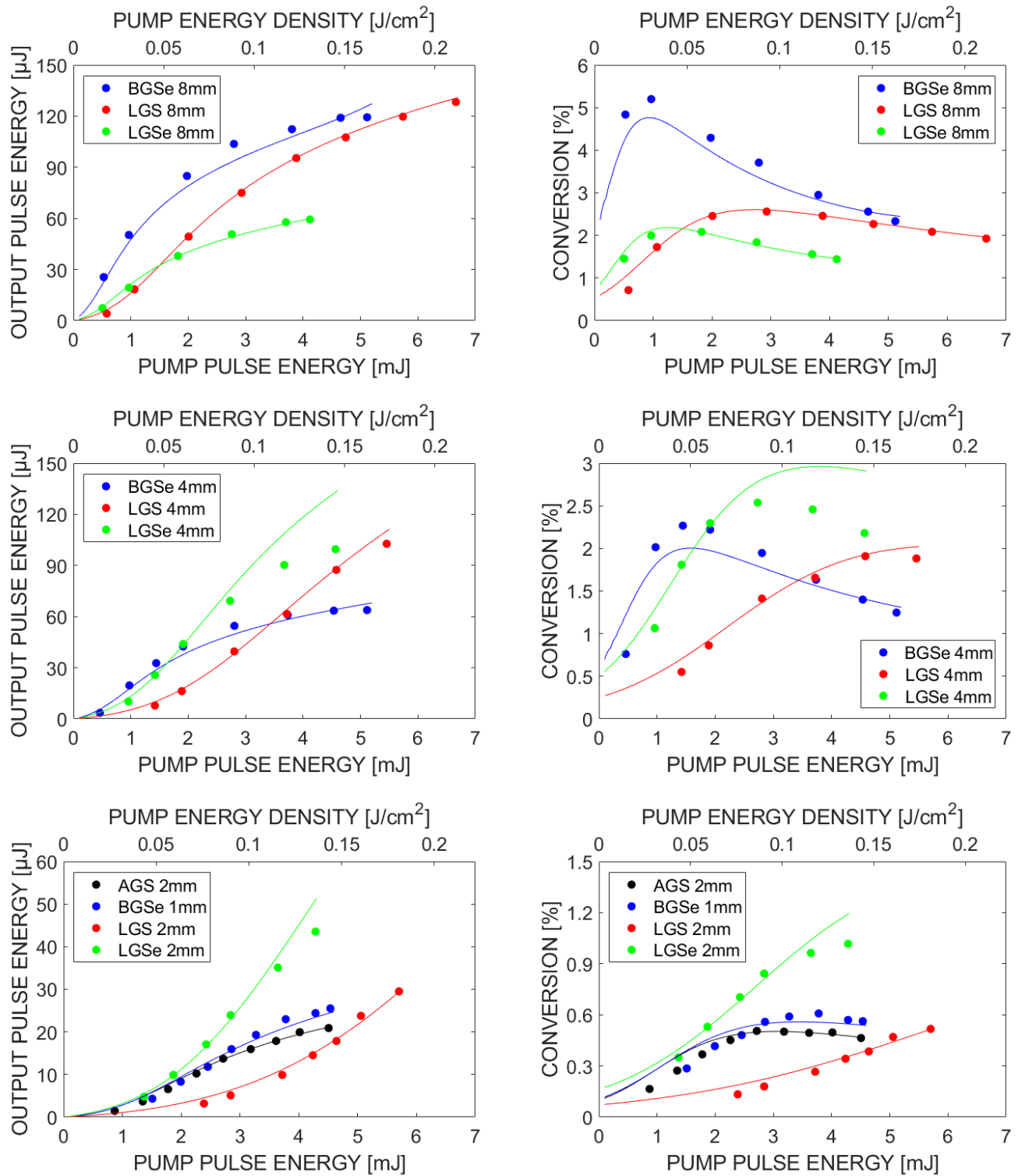


Fig. 4. Mid-IR  $\sim 7 \mu\text{m}$  output energy (left) and conversion efficiency (right) achieved with 8 mm long DFG crystals (top row), 4 mm long DFG crystals (middle row), and 1 or 2 mm long DFG crystals (bottom row). Points: measured data; line: numerical modeling.

REFERENCES

[1] K. L. Vodopyanov, *Laser-based Mid-infrared Sources and Applications*. Wiley, 2020.

[2] York, R. L. "A new optical parametric amplifier based on lithium thioindate used for sum frequency generation vibrational spectroscopic studies of the amide I mode of an interfacial model peptide," *Applied Spectroscopy* **2008**, 62, 938–940.

[3] Goya, K. "Stable 35-W Er:ZBLAN fiber laser with CaF<sub>2</sub> end caps," *Applied Physics Express* **2019**, 12, 102007.

[4] Sojka, L. "Experimental investigation of actively Q-switched Er<sup>3+</sup>:ZBLAN fiber laser operating at around 2.8  $\mu\text{m}$ ," *Sensors* **2020**, 20, 4642.

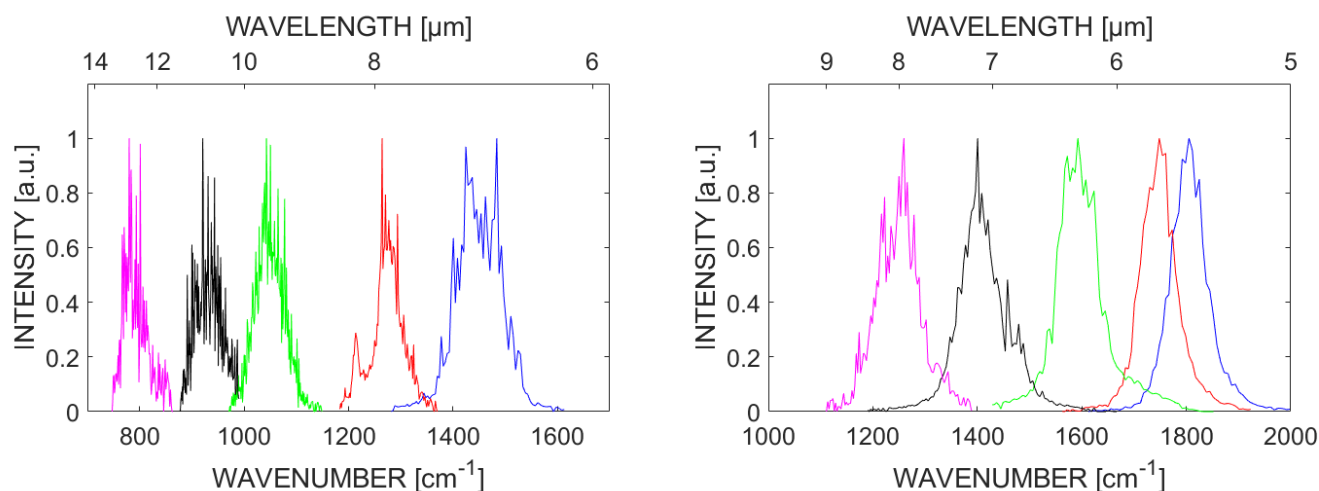


Fig. 5. DFG spectral tunability using the BGSe crystal (left) and LGS crystal (right) at high pump energy.

- [5] Jelinková, H. "Dysprosium thiogallate laser: source of mid-infrared radiation at 2.4, 4.3, and 5.4  $\mu\text{m}$ ," *Appl. Phys. A* **2016**, *122*, 738.
- [6] Martyskhin, D. "Room temperature, nanosecond, 60 mJ/pulse Fe:ZnSe master oscillator power amplifier system operating at 3.8-5.0  $\mu\text{m}$ ," *Optics Express* **2021**, *29*, 2387–2393.
- [7] Fjodorow, P. "Room-temperature Fe:ZnSe laser tunable in the spectral range of 3.7–5.3  $\mu\text{m}$  applied for intracavity absorption spectroscopy of  $\text{CO}_2$  isotopes, CO and  $\text{N}_2\text{O}$ ," *Opt. Express* **2021**, *29*, 12033–12048.
- [8] Doroshenko, M. E. "Room temperature  $\text{Fe}^{2+}:\text{Cd}_{1-x}\text{Mn}_x\text{Te}$  laser generating at 5.4–6  $\mu\text{m}$ ," *Opt. Letters* **2018**, *43*, 5058.
- [9] Frolov, M. P. "Tunable in the range of 4.5-6.8  $\mu\text{m}$  room temperature single-crystal Fe:CdTe laser pumped by Fe:ZnSe laser," *Opt. Express* **2020**, *28*, 17449–17456.
- [10] Pushkin, A. V. "Femtosecond graphene mode-locked Fe:ZnSe laser at 4.4  $\mu\text{m}$ ," *Opt. Letters* **2020**, *45*, 738.
- [11] Endo, M. *Gas lasers*, CRC Press, 2007.
- [12] Ionin, A. A. "Carbon monoxide laser emitting nanosecond pulses with 10 MHz repetition rate," *Opt. Commun.* **2009**, *282*, 294–299.
- [13] Brau, C. A. "Free-Electron Lasers," *Science* **1988**, *239*, 1115–1121.
- [14] Pecharrmán-Gallego, R. "An overview on quantum cascade lasers: origins and development," *Quantum Cascade Lasers*, Intech, 2017.
- [15] Slivken, S. "Surface emitting, tunable, mid-infrared laser with high output power and stable output beam," *Sci. Rep.* **2019**, *9*, 549.
- [16] Täschler, P. "Femtosecond pulses from a mid-infrared quantum cascade laser," *Nature Photonics* **2021**, *15*, 919–924.
- [17] Antognini, A. "Powerful fast triggerable 6  $\mu\text{m}$  laser for the muonic hydrogen 2S-Lamb shift experiment," *Opt. Commun.* **2005**, *253*, 362–374.
- [18] Petrov, V. "Frequency down-conversion of solid-state laser sources to the mid-infrared spectral range using non-oxide nonlinear crystals," *Progress in Quantum Electronics* **2015**, *42*, 1–106.
- [19] Leitenstorfer A. "The 2023 terahertz science and technology roadmap," *J. Phys. D: Appl. Phys.* **2023**, *56*, 223001.
- [20] Makhlof S. "Terahertz sources and receivers: From the past to the future," *IEEE J. of microwaves* **2023**, *3*, 894–912.
- [21] Insero, G. "Difference frequency generation in the mid-infrared with orientation-patterned gallium phosphide crystals," *Opt. Lett.* **2016**, *41*, 5114–5117.
- [22] Su, X. "Generation of 8–20  $\mu\text{m}$  Mid-Infrared Ultrashort Femtosecond Laser Pulses via Difference Frequency Generation," *Photonics* **2022**, *9*, 372.
- [23] Pires, H. "Ultrashort pulse generation in the mid-IR," *Progress in Quantum Electronics* **2015**, *43*, 1–30.
- [24] Smrž, M. "Advances in high-power, ultrashort pulse DPSSL technologies at HiLASE," *Appl. Sci.* **2017**, *7*, 1016.
- [25] Smith, A. V. mISNLO version 75 [Computer software] AS-Photonics.
- [26] Xu L. "Thulium-fiber-laser-pumped, high-peak-power, picosecond, mid-infrared orientation-patterned GaAs optical parametric generator and amplifier," *Opt. Letters* **2017**, *42*, 4036–4039.
- [27] Liu, Y. "High-power, high-repetition-rate tunable longwave mid-IR sources based on DFG in the OPA regime," *Opt. Letters* **2023**, *48*, 1052–1055.
- [28] Liu, P. "Widely tunable long-wave infrared difference frequency generation with a  $\text{BaGa}_4\text{Se}_7$  crystal," *Appl. Opt.* **2021**, *60*, 10984–10987.
- [29] Yang, F. "High-energy continuously tunable 8-14  $\mu\text{m}$  picosecond coherent radiation generation from BGSe-OPA pumped by 1064 nm laser," *Opt. & Laser Technol.* **2020**, *125*, 106040.
- [30] Yang, F. "High efficiency and high peak power picosecond mid-infrared optical parametric amplifier based on  $\text{BaGa}_4\text{Se}_7$  crystal," *Opt. Lett.* **2013**, *38*, 3903–3905.
- [31] Jelínek, M. "Difference frequency generation in  $\text{BaGa}_4\text{Se}_7$  tunable in a 6.5-8.5  $\mu\text{m}$  range with a peak power of 30 MW pumped by 1.03  $\mu\text{m}$ , 1.8 ps laser," *Optica High-brightness Sources and Light-driven Interactions Congress 2022*, Technical Digest Series (Optica Publishing Group, 2022), paper JTh4A.15.
- [32] Smetanin, S. N. "50- $\mu\text{J}$  level, 20-picosecond, narrowband difference-frequency generation at 4.6, 5.4, 7.5, 9.2, and 10.8  $\mu\text{m}$  in  $\text{LiGaS}_2$  and  $\text{LiGaSe}_2$  at Nd:YAG laser pumping and various crystalline Raman laser seeding," *Opt. Mater. Express* **2020**, *10*, 1881–1890.
- [33] Tian, K. "Mid-Infrared Few-Cycle Pulse Generation and Amplification," *Photonics* **2021**, *8*, 290.
- [34] Nakagawa, K. "Mid-infrared pulse generation using multi-plate white-light generation and optical parametric amplification in  $\text{LiGaS}_2$  crystals," *Applied Physics Express* **2023**, *16*, 032001.
- [35] Chen, B.-H. "Efficient middle-infrared generation in  $\text{LiGaS}_2$  by simultaneous spectral broadening and difference-frequency generation," *Opt. Lett.* **2018**, *43*, 1742–1745.
- [36] Bournet, Q. "Enhanced intrapulse difference frequency generation in the mid-infrared by a spectrally dependent polarization state," *Opt. Lett.* **2020**, *47*, 261–264.
- [37] Carnio, B.N. "Intra-pulse difference frequency generation in  $\text{ZnGeP}_2$  for high-frequency terahertz radiation generation," *Sci Rep* **2023**, *13*, 8161.
- [38] Yang, F. "Midinfrared optical parametric amplifier with 6.4-11  $\mu\text{m}$  range based on  $\text{BaGa}_4\text{Se}_7$  crystal," *IEEE Photon. Technol. Lett.* **2015**, *27*, 1100–1103.
- [39] Zhao, X. "Recalibration of the nonlinear optical coefficients of  $\text{BaGa}_4\text{Se}_7$  crystal using second-harmonic-generation method," *Opt. Lett.* **2021**, *46*, 5894–5897.
- [40] Guo, F. "Second-order nonlinear optical coefficients of the monoclinic crystal  $\text{BaGa}_4\text{Se}_7$ ," *Opt. Lett.* **2022**, *47*, 842–845.